JACC: BASIC TO TRANSLATIONAL SCIENCE VOL. 6, NO. 8, 2021

PRECLINICAL RESEARCH

Selective FPR2 Agonism Promotes a Proresolution Macrophage Phenotype and Improves Cardiac Structure-Function Post Myocardial Infarction

Ricardo A. García, PHD,[a,b] John A. Lupisella, MSC,[a] Bruce R. Ito, PHD,[b] Mei-Yin Hsu, MSC,[a] Gayani Fernando, MSC,[a] Nancy L. Carson, BSC,[a] John J. Allocco, BSC,[a] Carol S. Ryan, BSC,[a] Rongan Zhang, MSC,[a] Zhaoqing Wang, MSC,[a] Madeleine Heroux, PHD,[c] Marilyn Carrier, PHD,[c] Stéphane St.-Onge, MSC,[c] Michel Bouvier, PHD,[c] Shailesh Dudhgaonkar, PHD,[d] Jignesh Nagar, MSC,[d] Moises M. Bustamante-Pozo, PHD,[b] Alejandra Garate-Carrillo, PHD,[b] Jian Chen, PHD,[a] Xiuying Ma, PHD,[a] Debra J. Search, BSC,[a] Elizabeth A. Dierks, PHD,[a] Ellen K. Kick, PHD,[a] Ruth R. Wexler, PHD,[a] David A. Gordon, PHD,[a] Jacek Ostrowski, PHD,[a] Nicholas R. Wurtz, PHD,[a] Francisco Villarreal, MD, PHD[b]

VISUAL ABSTRACT

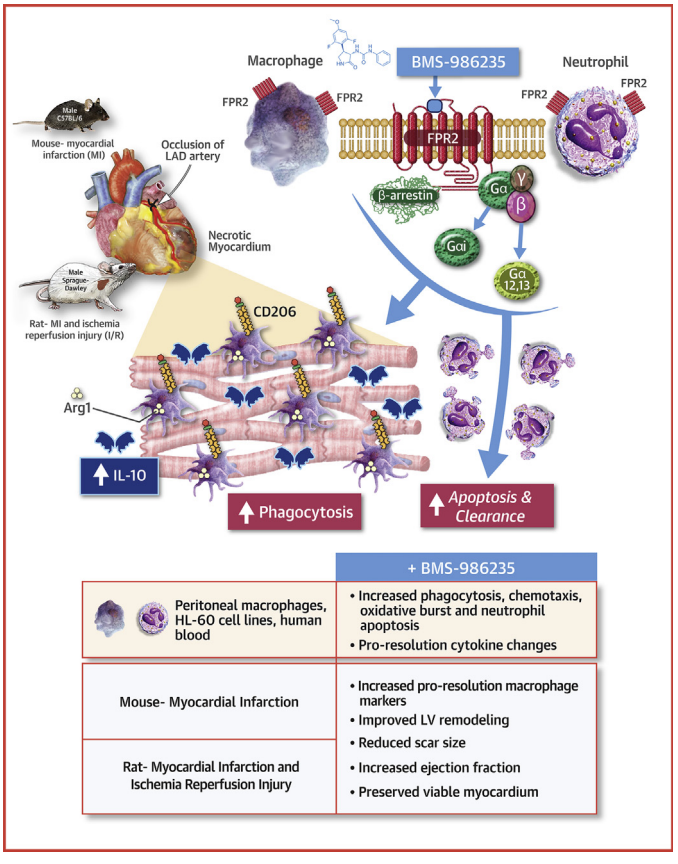

García, R.A. et al. J Am Coll Cardiol Basic Trans Science. 2021;6(8):676-689.

HIGHLIGHTS

- MI leads to ischemic damage of myocardium and activation of inflammatory programs as part of the wound healing response.
- Selective activation of FPR2 on macrophages potentiates key cellular activities that enable wound healing.
- MI was induced in rodents to study the effects of treatment with BMS-986235, a selective small molecule agonist of FPR2.
- BMS-986235 stimulated proresolution macrophage activities, induced neutrophil apoptosis and clearance, improved LV and infarct structure, and preserved cardiac function post MI.
- The findings suggest that targeted activation of FPR2 can improve post-MI outcome and may diminish the development of HF.

ISSN 2452-302X https://doi.org/10.1016/j.jacbts.2021.07.007

SUMMARY

Dysregulated inflammation following myocardial infarction (MI) leads to maladaptive healing and remodeling. The study characterized and evaluated a selective formyl peptide receptor 2 (FPR2) agonist BMS-986235 in cellular assays and in rodents undergoing MI. BMS-986235 activated G proteins and promoted β-arrestin recruitment, enhanced phagocytosis and neutrophil apoptosis, regulated chemotaxis, and stimulated interleukin-10 and monocyte chemoattractant protein-1 gene expression. Treatment with BMS-986235 improved mouse survival, reduced left ventricular area, reduced scar area, and preserved wall thickness. Treatment increased macrophage arginase-1 messenger RNA and CD206 receptor levels indicating a proresolution phenotype. In rats following MI, BMS-986235 preserved viable myocardium, attenuated left ventricular remodeling, and increased ejection fraction relative to control animals. Therefore, FPR2 agonism improves post-MI healing, limits remodeling and preserves function, and may offer an innovative therapeutic option to improve outcomes. (J Am Coll Cardiol Basic Trans Science 2021;6:676–689)

ABBREVIATIONS AND ACRONYMS

BRET = bioluminescence resonance energy transfer

EC_{50} = half maximal effective concentration

FPR2 = formyl peptide receptor 2

HF = heart failure

IL = interleukin

I/R = ischemia-reperfusion

KO = knockout

LV = left ventricle/ventricular

LPS = lipopolysaccharide

MCP = monocyte chemoattractant protein

MI = myocardial infarction

mRNA = messenger RNA

SAA = serum amyloid A

TNF = tumor necrosis factor

WT = wild-type

The inflammatory response is essential for cardiac healing following myocardial infarction (MI). Dysregulated and unresolved inflammation has been recognized as a major mechanism responsible for the development of heart failure (HF) and, eventually, mortality (1). Treatments focused on inhibiting proinflammatory mediators have been unsuccessful in preventing the development of HF post MI. Some notable examples of these failed approaches include treatment with glucocorticoids (2,3), and inhibitors of cyclooxygenase-2 (4) and tumor necrosis factor (TNF)-α (5). Adverse events with glucocorticoids included left ventricular (LV) wall rupture and increased mortality with cyclooxygenase-2 or TNF-α inhibition. These outcomes led to the concept that instead of broadly inhibiting inflammation, the stimulation of resolution could provide a safe and effective approach to limit tissue damage and facilitate healing after an acute injury such as a MI. The discovery of proresolution mediators such as lipoxins, resolvins, and maresins, as well as the identification of proresolution receptors such as the formyl peptide receptor 2 (FPR2), has led to new insights toward addressing unresolved inflammation (6).

FPR2 is a G protein-coupled receptor expressed by phagocytic leukocytes, including macrophages, and plays an important role in the initiation and resolution of inflammation (6). These distinct functions are regulated by specific ligands to evoke unique leukocyte responses. For example, polypeptide ligands such as serum amyloid A (SAA) and damage associated molecular pattern peptides binding to FPR2 trigger a proinflammatory signaling cascade. These chemotactic signals recruit leukocytes to a site of infection, tissue damage, or ongoing inflammation. By contrast, endogenous small lipid molecules derived from arachidonic acid (lipoxin A4) or from omega-3 docoshexaenoic acid (resolvin D1) trigger distinct pharmacological responses that stimulate resolution of inflammation. These ligands can polarize blood-derived and tissue-resident macrophages toward a proresolution or pro-wound healing phenotype, sometimes referred to as "M2" (7). The phenotypic switch prevents macrophage apoptosis and enhances the efferocytosis of apoptotic neutrophils and cellular debris from damaged necrotized tissue, leading to termination of inflammation and the initiation of resolution and wound healing (8).

From the [a]Department of Cardiovascular and Fibrosis Drug Discovery, Bristol Myers Squibb, Princeton, New Jersey, USA; [b]Department of Medicine, University of California-San Diego, San Diego, California, USA; [c]Institute for Research in Immunology and Cancer, Université de Montréal, Montreal, Quebec, Canada; and the [d]Biocon Bristol Myers Squibb Research Center, Bangalore, India.

Michael R. Bristow, MD, PhD, served as the Guest Editor-in-Chief for this paper.

The authors attest they are in compliance with human studies committees and animal welfare regulations of the authors' institutions and Food and Drug Administration guidelines, including patient consent where appropriate. For more information, visit the Author Center.

Manuscript received March 30, 2021; revised manuscript received July 20, 2021, accepted July 20, 2021.

Endogenously derived ligands of FPR2 such as lipoxin A4 and resolvin D1 are relatively unstable (9,10) and therefore not suitable for use as pharmacological agents to stimulate resolution of inflammation. Studies with dual FPR2/FPR1 small molecule agonists demonstrated cardioprotection in preclinical models of MI (11,12). Although these studies did not show overt FPR1-mediated derangements in proresolution function with FPR1 activation, the findings suggested a prominent role for FPR2 over FPR1 in mediating these responses (11). Therefore, we hypothesized that selective activation of FPR2 may be more effective in driving proresolution activity of macrophages to potentiate post-MI wound healing.

BMS-986235 (also known as LAR-1219) is a potent, selective, and orally bioavailable agonist of FPR2 (13). Initial studies with BMS-986235 suggested the potential to improve cardiac structure when given post MI in the mouse (13). In the present series of experiments, we evaluated the proresolution properties of BMS-986235 and its capacity to improve cardiac structure-function outcome post MI in several well-established and translational rodent MI models.

METHODS

For experimental methods describing in vitro and cellular assays and detailed in vivo methods, please refer to the Supplemental Appendix.

ANIMAL STUDIES. Animal studies were carried out in accordance with guidelines set by Bristol Myers Squibb and University of California San Diego Animal Care and Use Committees. Adult male C57BL/6 mice (10-12 weeks old) and adult male Sprague Dawley rats (6-7 weeks old) were purchased from the Jackson Laboratory (Bar Harbor, Maine) and Charles River Laboratories (Wilmington, Massachusetts), respectively.

MYOCARDIAL INFARCTION. Animals were anesthetized with an intraperitoneal injection of ketamine (100 mg/kg) and xylazine (8 mg/kg) followed by endotracheal intubation and mechanical ventilation with oxygen supplemented with isoflurane (2.0%-2.5%). The heart was exposed via a left thoracotomy. In mice and rats, the left anterior descending artery was occluded by suture.

TERMINAL HEMODYNAMICS AND EX VIVO PRESSURE VOLUME STUDIES. In rat terminal experiments 6 weeks post MI, animals were anesthetized with isoflurane and a transducer-tipped conductance catheter (2.5-F, Millar) was inserted into the LV via a right carotid cutdown. LV pressure-volume loop data were acquired and corrected for parallel conductance. Rat hearts from ischemia-reperfusion (I/R) experiments were arrested in diastole, removed, and mounted on a modified Langendorff apparatus for determination of ex vivo passive LV pressure-volume relationships.

DATA AND STATISTICS. Data are presented in the text and supplemental tables using the mean ± SD; data in bar and line graphs are shown as mean ± SEM. Comparisons between groups were evaluated using Student's *t* test or 1-way analysis of variance followed by Dunnett's post hoc test for multiple pairwise comparisons. The log-rank test was used to compare survival curves between groups 0 to 28 days post MI. Reported half maximal effective concentration (EC_{50}) values represent compound concentrations that stimulate a half maximal response determined using a nonlinear concentration response curve. For studies using isolated human blood, each data point depicted in the scatterplots represents the mean of at least triplicate measurements per donor. GraphPad Prism Version 8.4.1 (GraphPad Software, San Diego, California) was used for all statistical and curve fit analyses. Statistical significance was noted as $P < 0.05$, $P < 0.01$, or $P < 0.001$.

RESULTS

The signaling profile of BMS-986235 was examined in HEK293 cells transiently expressing human FPR1 or FPR2 (**Figure 1**). BMS-986235 produced concentration-dependent modulation of bioluminescence resonance energy transfer (BRET) signals for Gαi1, Gαi2, Gαi3, GαoA, and GαoB biosensors following FPR1 and FPR2 activation (EC_{50} shown in **Figures 1A to 1E**). The response was FPR2-selective relative to FPR1 with selectivity ratios (FPR2 EC_{50}/FPR1 EC_{50}) ranging 164- to 614-fold. A highly selective response was observed for Gα12 and Gα13 biosensors after stimulation of FPR1- or FPR2-expressing cells with BMS-986235 (**Figures 1F and 1G**). A concentration-dependent increase in the BRET signal was observed for Gα12 and Gα13 in FPR2-expressing cells, whereas minimal to no increase was observed in FPR1-expressing cells. A similar FPR2-selective response was obtained for β-arrestin1 and 2 recruitment (**Figures 1H and 1I**). The comprehensive profiles shown in **Figure 1** demonstrate the FPR2-selective properties of BMS-986235 across multiple signaling pathways. These results are consistent with the human FPR2 selectivity profile of BMS-986235 obtained via activation of FPR2 Gi coupling and downstream cAMP inhibition (FPR2 EC_{50} = 5 nM; FPR1 EC_{50} = 400 nM) (Supplemental Table 1) (13). In addition, BRET assays were carried out using rat and mouse FPR2 receptors, which

FIGURE 1 Signaling Profile of BMS-986235 in HEK293 Cells Expressing Human FPR2 and FPR1

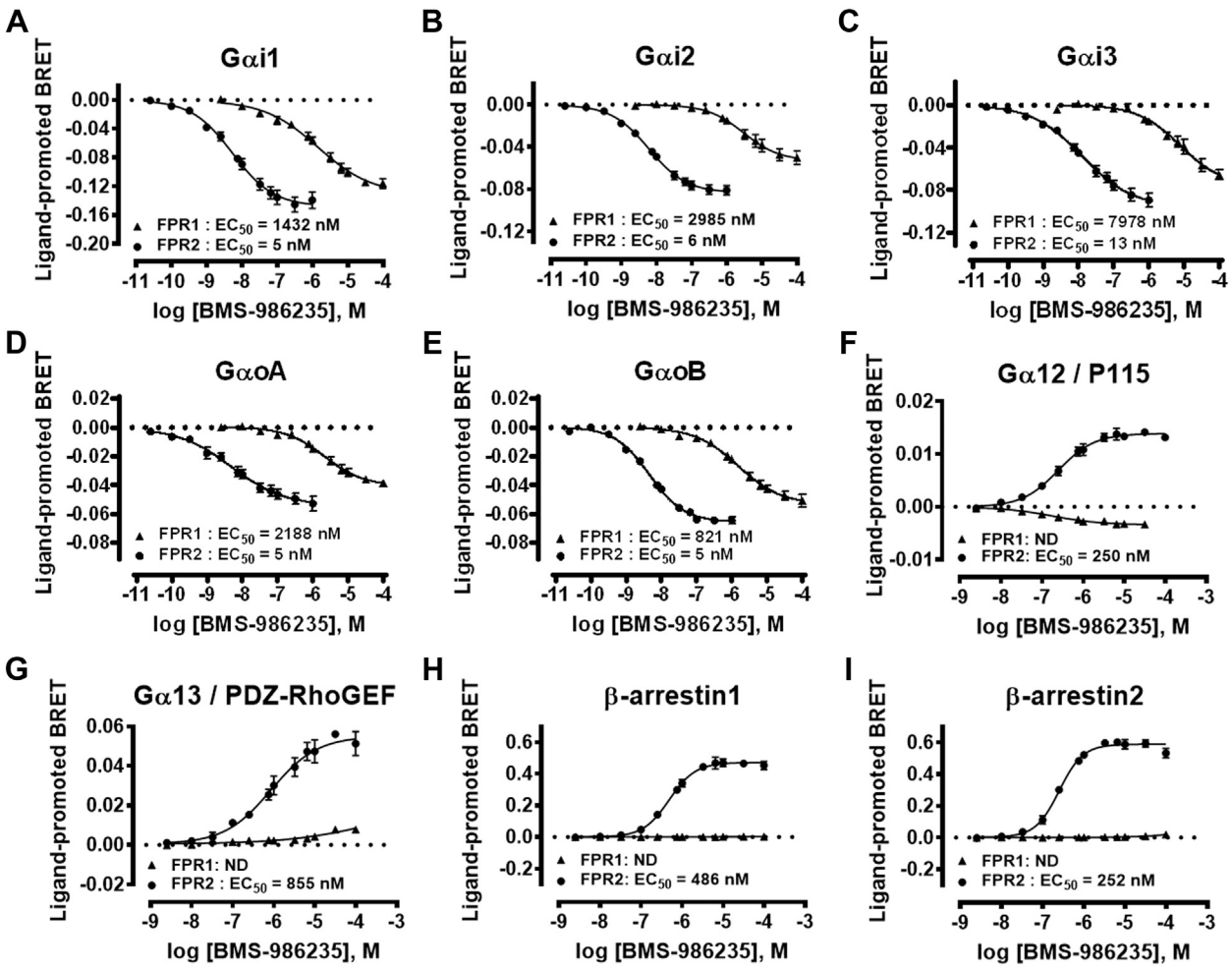

The ability of BMS-986235 to engage different signaling pathways was assessed using bioluminescence resonance energy transfer (BRET) biosensors detecting the activation of **(A)** Gαi1 **(B)** Gαi2, **(C)** Gαi3, **(D)** GαoA, and **(E)** GαoB; the interaction of effectors with **(F)** Gα12 and **(G)** Gα13; and the recruitment of **(H)** β-arrestin1 and **(I)** and β-arrestin2 to the plasma membrane. HEK293 cells expressing human formyl peptide receptor 2 (FPR2) or FPR1 were stimulated with BMS-986235, and modulation of the BRET signals from the different biosensors was recorded. Data represent the mean ± SEM of 3 independent experiments. ND = not determined.

confirmed FPR2 activation of the Gi pathway as well as recruitment of β-arrestin1 to rodent FPR2 with BMS-986235 (Supplemental Figure 1). Moreover, the selectivity profile of BMS-986235 observed with human FPR2 was confirmed using mouse and rat FPR orthologs in the cAMP assay (Supplemental Table 1). Overall, the signaling profile of BMS-986235 was conserved across species after stimulation with the agonist.

Zymosan phagocytosis was evaluated in peritoneal macrophages from wild-type (WT), FPR1 knockout (KO), and FPR2 KO mice. As shown in **Figure 2A**, potent stimulation of phagocytosis with BMS-986235 occurred with WT-derived macrophages (EC_{50} = ~8 pM) with a Ymax approaching 100%. By contrast, FPR2 KO-derived macrophages showed a minimal response to BMS-986235 above the control macrophages. FPR1 KO-derived macrophages, showed a response that resembled WT (EC_{50} = ~2 pM), which is consistent with the selectivity profile of BMS-986235 and the importance of FPR2 for phagocytosis activity.

Phagocytes respond to chemotactic stimuli and degrade internalized particles and bacteria while undergoing an oxidative respiratory burst. Stimulation of oxidative burst activity and chemotaxis was investigated using differentiated human promyelocytic leukemia HL-60 cells, which possess a neutrophil-like lineage and endogenously express

FIGURE 2 Regulation of Inflammatory Cell Function by BMS-986235

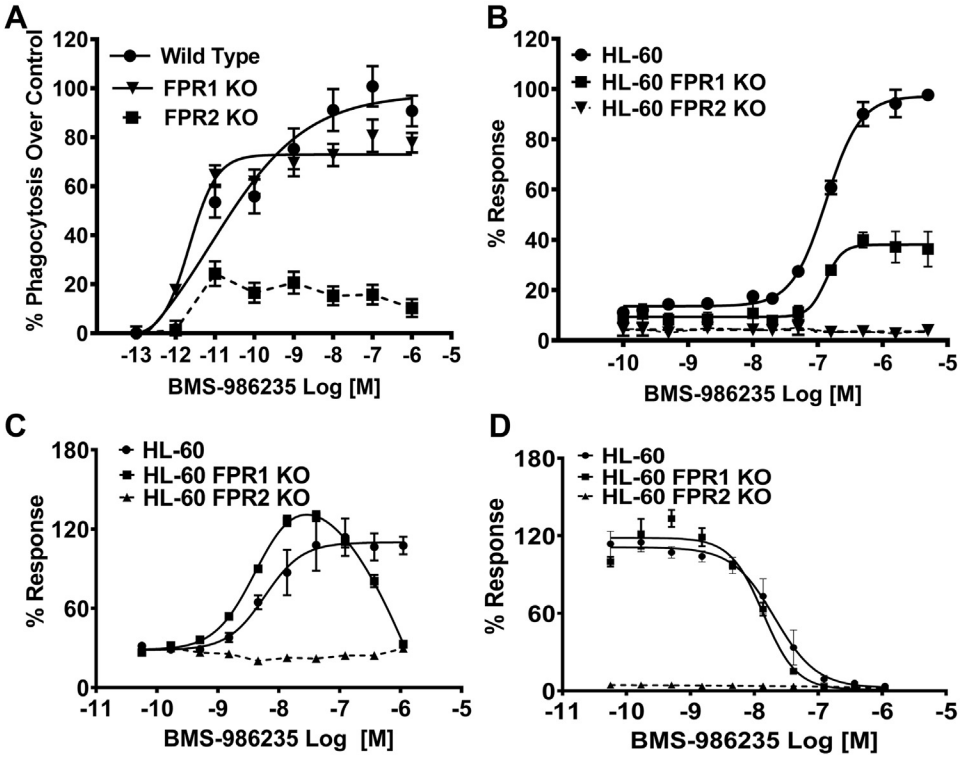

(A) Enhancement of zymosan phagocytosis by BMS-986235 was assessed in BioGel-elicited peritoneal macrophages from wild-type, FPR1 knockout (KO), and FPR2 KO mice. **(B)** Stimulation of oxidative burst activity was evaluated in neutrophil-like HL-60, HL-60 FPR1 KO, and HL-60 FPR2 KO cell lines. **(C)** Chemotactic responses to BMS-986235 were evaluated in differentiated HL-60, HL-60 FPR1 KO, and HL-60 FPR2 KO cell lines. **(D)** Inhibition of chemotaxis toward serum amyloid A by BMS-986235. Curves were fit using least squares method of nonlinear regression (GraphPad Prism).The half maximal effective concentration (EC_{50}) value for the HL-60 FPR1 KO data shown in **C** assumed a bell-shaped curve and was calculated from the stimulatory phase of the response. **Dotted lines** indicate no curve fit. Data represent the mean ± SEM of 3 independent experiments.

FPR1 and FPR2 (11,14). HL-60 cells that express both receptors showed a robust oxidative burst response when stimulated with BMS-986235 (EC_{50} = 130 nM, Ymax = 97%) (**Figure 2B**). Activity was abolished in the HL-60 FPR2 KO line. Interestingly, in the HL-60 FPR1 KO line, BMS-986235 stimulated an attenuated maximal response (Ymax = 38%) but with a similar potency as the parenteral HL-60 cell line (EC_{50} = 130 nM). These data suggest an indirect role of FPR1 in oxidative burst activity that may be required to drive maximal activity with BMS-986235.

BMS-986235 stimulated the in vitro chemotactic response of differentiated HL-60 cells with an EC_{50} value of 6 nM (**Figure 2C**). A prochemotactic response was obtained with HL-60 cells deficient in FPR1 (EC_{50} = 4 nM) for a greater portion of the concentration response curve. However, attenuation was observed at higher BMS-986235 concentrations (>120 nM) yielding a bell-shaped response. Similar chemotaxis patterns have been observed in HL-60 cells treated with prochemotactic peptide agonists of FPR2 (15). In the HL-60 FPR2 KO line, no enhancement in chemotaxis with BMS-986235 was obtained. When HL-60 cells were pretreated with BMS-986235, chemotaxis toward serum amyloid A (SAA), a potent proinflammatory apolipoprotein and a known ligand for FPR2 (16), was inhibited with a half maximal inhibitory concentration value of 21 nM. A similar antagonist profile was obtained with FPR1-deficient HL-60 cells (half maximal inhibitory concentration = 14 nM). By contrast, with HL-60 FPR2 KO cells, chemotaxis toward the FPR2 ligand SAA was not detected.

BMS-986235 stimulated the concentration-dependent gene expression of the proresolution cytokine interleukin (IL)-10 in isolated human whole blood (**Figure 3A**). On average, the increases in

FIGURE 3 In Vitro mRNA Expression of Cytokines and FPR2 in Isolated Human Blood

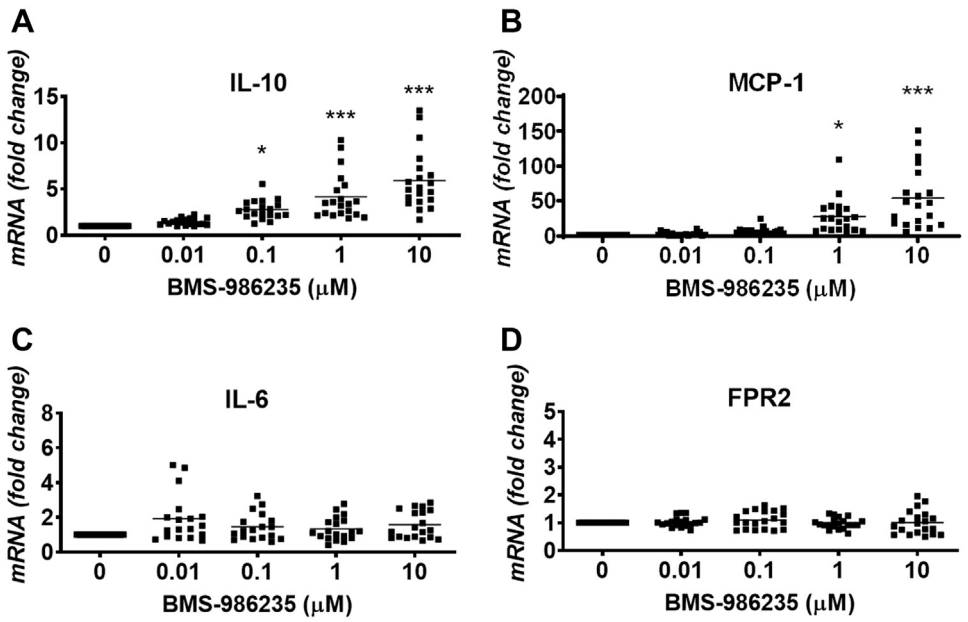

(A) Interleukin (IL)-10, **(B)** monocyte chemoattractant protein (MCP)-1, **(C)** IL-6, and **(D)** formyl peptide receptor 2 (FPR2). Whole blood from 20 consenting donors was processed as described in the Supplemental Material and Methods. Each data point represents the mean of at least triplicate measurements per donor. The mean value is depicted by the solid line relative to the distribution of data points for each concentration. Dunnett's vs vehicle: *$P < 0.05$, ***$P < 0.001$. mRNA = messenger RNA.

messenger RNA (mRNA) levels ranged from 3-fold at 0.1 μM BMS-986235 to 6-fold at 10 μM BMS-986235. Incubation with BMS-986235 also induced concentration-dependent increases in monocyte chemoattractant protein (MCP)-1 of 28- and 54-fold versus control at 1 and 10 μM concentrations, respectively (**Figure 3B**). By contrast, no significant induction of IL-6, IL-8, TNFα (**Figure 3C,** Supplemental Figure 2), or FPR2 (**Figure 3D**) was detected at any concentration of BMS-986235.

Potentiation of neutrophil apoptosis by BMS-986235 was evaluated using isolated human neutrophils activated with SAA. SAA is known to prolong the lifespan of proinflammatory neutrophils and augments tissue damage associated with neutrophil dysregulation (17). Promotion of neutrophil apoptosis thereby diminishes proinflammatory neutrophil damage and leads to apoptotic cell removal and inflammation resolution (18-20). As shown in **Figure 4**, SAA exposure increased the percentage of viable neutrophils by 18% relative to dimethyl sulfoxide control while decreasing the amount of apoptotic and dead neutrophils by 7% in both cases. By contrast, co-incubation of neutrophils with BMS-986235 and SAA reduced the percentage of viable neutrophils by 12% relative to SAA-only treatment and increased apoptotic cells by 11%. Representative flow cytometry plots for apoptotic and viable neutrophils are provided (Supplemental Figure 3).

The effects of early short-term treatment with BMS-986235 on infarct collagen and cardiac inflammation were evaluated in mouse myocardial tissue ~3 days following MI. The dose of BMS-986235 (3 mg/kg; once a day by oral gavage started 24 hours post MI) was chosen based on IL-10 release in noninfarcted mice following challenge with lipopolysaccharide (LPS) (**Figure 5A**), in which circulating IL-10 increased maximally at the 3 mg/kg dose (5.3-fold vs vehicle; $P < 0.001$). Infarct size measured 3 days post MI was similar between BMS-986235 and vehicle treatments (**Figure 5B**). Histology revealed increased collagen content within the infarct (**Figure 5C**) and a trend toward decreased infarct MMP-2 levels via immunohistological staining (**Figure 5D**). In situ hybridization detection showed increases in arginase-1 mRNA within the peri-infarct border zone with BMS-986235 treatment (+6.4 fold vs vehicle; $P < 0.05$) (**Figures 5E and 5F**). Representative histology images are provided in Supplemental Figures 4 and 5.

FIGURE 4 Apoptosis of Isolated Human Neutrophils

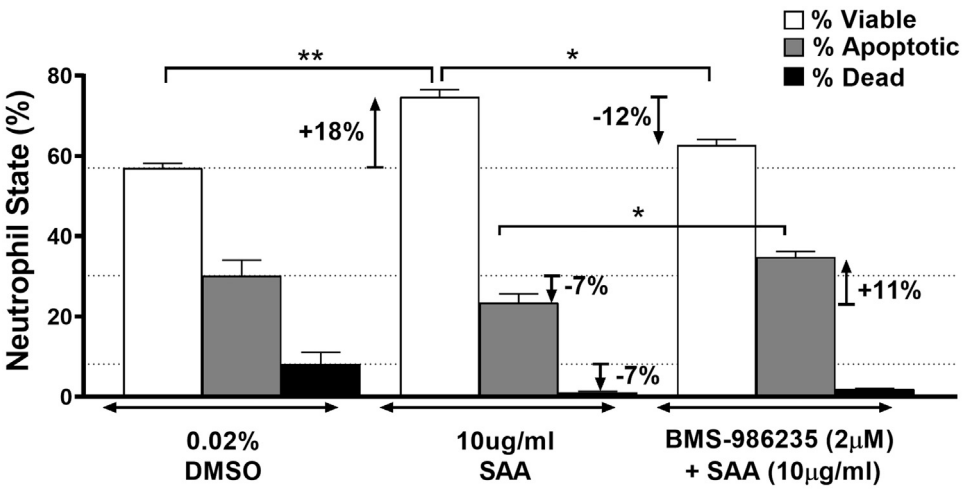

Neutrophils were incubated with dimethyl sulfoxide (DMSO) (0.02%), serum amyloid A (SAA) (10 μg/mL), or the combination of BMS-986235 (2 μM, 15-minute pretreatment) and SAA (10 μg/mL). The relative ratios of viable, apoptotic, and dead cells were determined for each treatment condition using annexin V and propidium iodide staining followed by flow cytometry. The **dashed lines** depict the mean of viable, apoptotic, and dead neutrophils for DMSO reference control. Data represent the mean ± SEM. *$P < 0.05$, **$P < 0.01$, unpaired t test.

A comparative experiment using the same in life protocol was carried out to evaluate global changes in cardiac macrophages and neutrophils via flow cytometry with a gating strategy for cell identification (**Figure 6A,** Supplemental Figure 6). To assess polarization of macrophages by BMS-986235, infarcted hearts were analyzed 3 days post left coronary artery occlusion. The numbers of total leukocytes (**Figure 6B**) and total macrophages (**Figure 6C**) were unchanged relative to infarcted mice treated with vehicle. However, the fraction of macrophages expressing CD206 ("M2") was increased significantly (**Figure 6D**). CD206 binds proinflammatory glycoproteins such as myeloperoxidase and mediates their clearance (21). As such, CD206 expression is low during inflammation and is high during resolution. Cell surface expression of CD206 is therefore a well-recognized early marker of macrophage polarization from a proinflammatory phenotype to a proresolution or reparative phenotype. A concomitant reduction in the percentage of CD206-negative macrophages ("M1") was also observed (**Figure 6E**). In addition, total neutrophil numbers were reduced suggesting an increased clearance rate with BMS-986235 treatment (**Figure 6F**). Absolute cell numbers for these various parameters are also provided (Supplemental Figure 7). Taken together, these results are consistent with the concept that FPR2 drives neutrophil apoptosis and accelerates phagocytic clearance by macrophages (18-20). Moreover, immunohistochemical analysis of myocardial CD206 and IL-10 levels at the peri-infarct zone of rats early post infarction (5 days post-artery ligation) showed relative increases with BMS-986235 treatment versus vehicle (Supplemental Figure 8).

The effects of a 28-day treatment regimen with BMS-986235 (0.3 and 3 mg/kg once a day by oral gavage) on LV and infarct scar remodeling were evaluated in the mouse permanent coronary artery occlusion model. Treatment with BMS-986235 led to a significant reduction in mortality over the 4 week study at the 3 mg/kg dose (**Figure 7A**). **Figure 7B** shows representative trichrome-stained LV sections (mid-ventricle). Following MI, a significant thinning and distention of the LV cavity is noted. With BMS-986235 treatment, scar area was reduced and infarct wall thickness and LV chamber area were preserved. The histomorphometric values for these changes are summarized in **Figure 7**, in which LV % scar area (**Figure 7C**), infarct wall thickness (**Figure 7D**), and LV chamber area (**Figure 7E**) are reported.

The capacity of BMS-986235 to improve infarct scar remodeling and LV structure-function relationships post MI was also evaluated in the rat via permanent coronary artery occlusion and I/R injury. Similar to the mouse studies, the dose of BMS-986235 used in the rat MI studies (1 mg/kg) corresponded to an efficacious dose for IL-10 induction in noninfarcted rats

FIGURE 5 Acute IL-10 Response and Post-MI Infarct Phenotype in Mouse

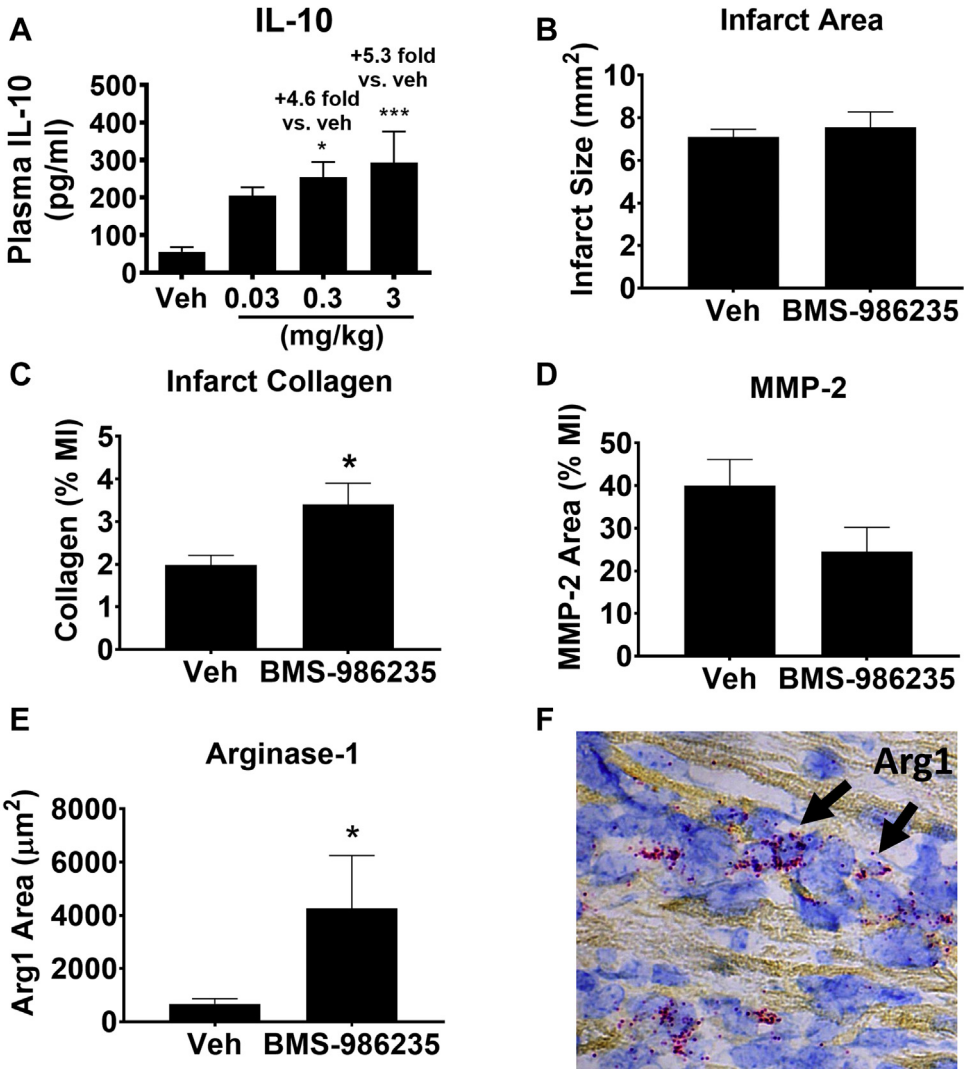

(A) Dose-dependent increase in interleukin (IL)-10 protein with BMS-986235 pretreatment (0.03, 0.3, or 3 mg/kg; n = 8 per group) and challenge with lipopolysaccharide. Histological measurements of **(B)** infarct area, **(C)** infarct collagen, and **(D)** infarct matrix metalloproteinase-2 (MMP-2) 74 hours following myocardial infarction (MI) and treatment with vehicle (Veh) or BMS-986235 (3 mg/kg; n = 8/group). **(E)** Detection and quantification of arginase-1 messenger RNA (mRNA) levels in the peri-infarct zone by in situ hybridization for Veh and BMS-986235 treatment groups (3 mg/kg; n = 4 per group). **(F)** Representative image of the peri-infarct zone from infarcted mice treated with BMS-986235 (3 mg/kg). Arginase-1 (Arg1) mRNA is indicated in **red** and FPR2 mRNA is indicated in **blue**. Data represent the mean ± SEM. Statistical comparisons were done with an unpaired *t* test or a Dunnett's test vs Veh when comparing multiple dose groups: $*P < 0.05$, $***P < 0.001$.

challenged with LPS (Supplemental Figure 9). Treatment with BMS-986235 reduced scar area and preserved infarct wall thickness versus vehicle (-26% and +38%; $P < 0.01$) (**Figures 8A and 8B**). BMS-986235 attenuated post-MI LV remodeling as indicated by reduction in LV end-diastolic and end-systolic volumes measured by echocardiography (-26% and -29% vs vehicle; $P < 0.01$) (**Figures 8C and 8D,** Supplemental Figure 10). BMS-986235 treatment increased ejection fraction by 46% versus vehicle ($P < 0.001$) (**Figure 8E**). Importantly, this activity was also present in the model of myocardial I/R. Treatment

FIGURE 6 Cardiac Inflammation and CD206+ Macrophage Levels Post MI in Mouse

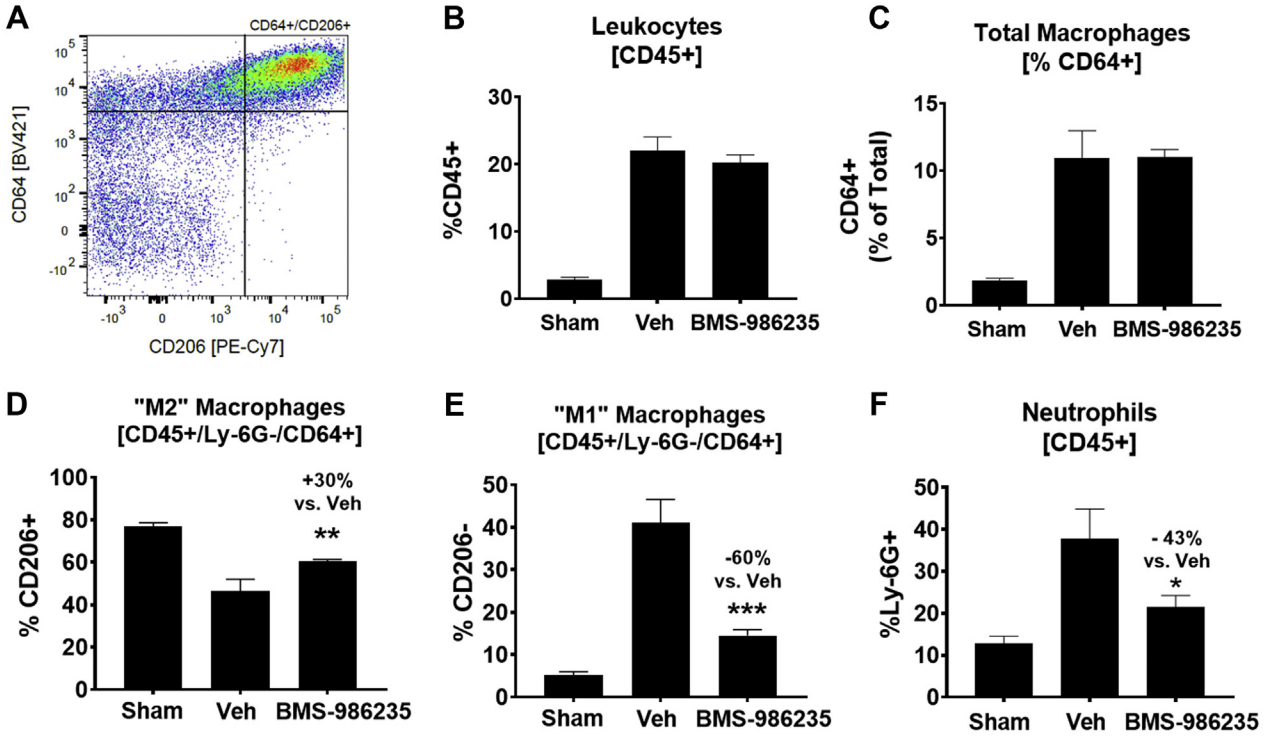

Analysis of total leukocytes, neutrophils, and macrophage polarization status in the heart following myocardial infarction (MI) by flow cytometry. **(A)** Representative bivariate plot of final gate for CD206+ macrophage population. **(B)** Total CD45+ leukocytes, **(C)** % of total CD45+ leukocytes that are CD64+ monocyte/macrophages, **(D)** % of CD64+ monocyte/macrophages that are CD206+ ("M2"), **(E)** % of CD64+ monocyte/macrophages that are CD206- ("M1"), and **(F)** % of total CD45+ leukocytes that are Ly6G+ neutrophils. Treatments consisted of vehicle (Veh) (n = 7) or 3 mg/kg BMS-986235 (n = 10). Noninfarcted sham hearts (n = 10) are shown for comparison. Data represent the mean ± SEM. T-test vs Veh: $*P < 0.05$, $**P < 0.01$, $***P < 0.001$.

with BMS-986235 reduced LV volumes by 26% and 42% at end-diastole and end-systole, respectively ($P < 0.01$) (Figures 8F and 8G). Moreover, the ex vivo LV pressure-volume curve obtained with BMS-986235 was left shifted from vehicle and approached the profile obtained with noninfarcted sham rats, indicating smaller LV chamber volumes versus vehicle (Figure 8H). BMS-986235 increased LV ejection fraction by 32% ($P < 0.01$) (Figure 8I). Histological examination of infarct structure showed that BMS-986235 increased viable myocardium across the infarct wall from epicardium to endocardium (Figure 8J). This effect was evident throughout the length of the infarct and occurred without altering the transmural thickness of the infarct wall relative to vehicle treatment (Supplemental Figure 11). Regional measurements revealed increases of 31% in proximal and mid MI regions ($P < 0.05$) and a trend toward increased viable myocardium at the distal end of the MI (Figure 8K). Summary tables describing the various LV function parameters measured by terminal hemodynamics methods in both rat MI studies are provided in the Supplemental Appendix (Supplemental Tables 2 and 3). Moreover, blood compound levels for the various rodent studies are also provided (Supplemental Table 4). For all in vivo experiments, compound levels were measured between 1.5 to 3 hours post dosing. At these measured times, total blood compound concentrations were above the EC_{50} values of cAMP responses stimulated by BMS-986235 for mouse or rat FPR2 (Supplemental Table 1). Moreover, the free fraction of BMS-986235 in blood for mouse (9%) and rat (13%) at least approximated the rodent cAMP-derived EC_{50} values.

DISCUSSION

Unmitigated adverse cardiac remodeling after MI leads to ventricular dysfunction and progression to HF. Despite advances in therapies and interventional

FIGURE 7 Effects of BMS-986235 on Post-Infarction Structure-Function in Mouse

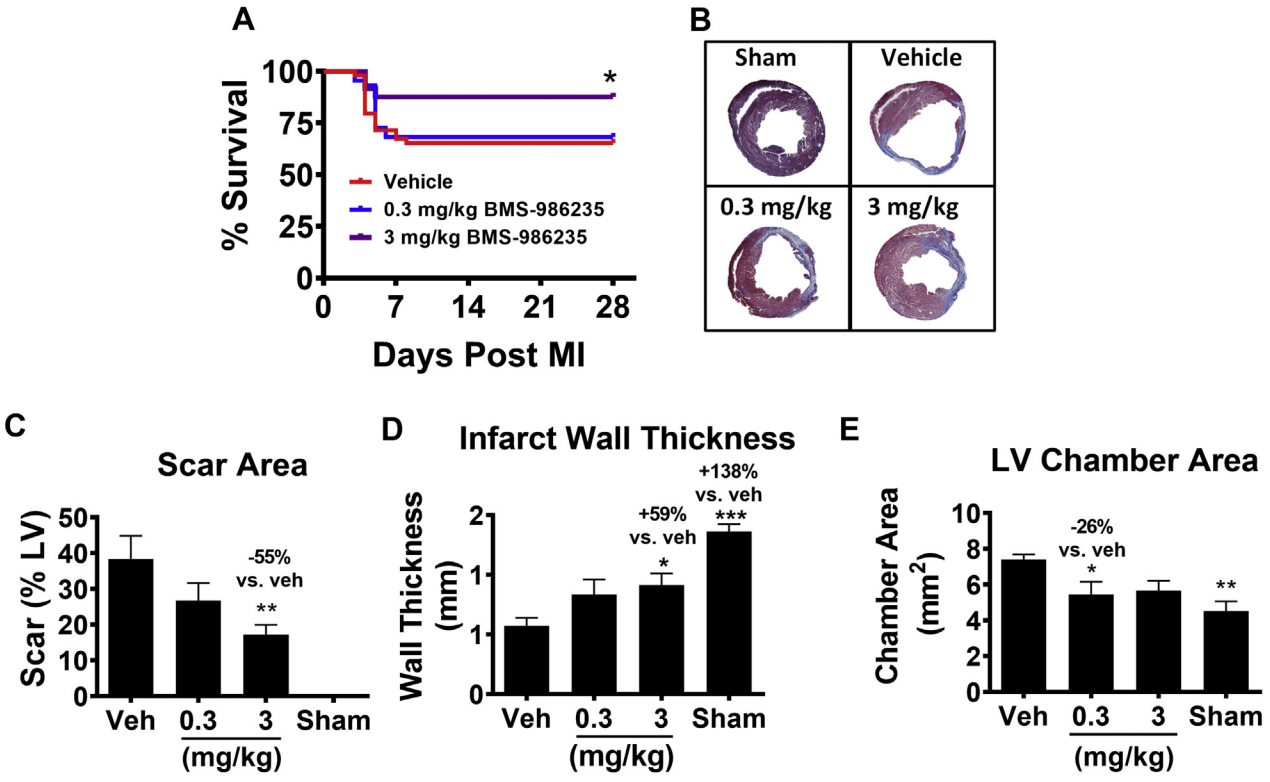

Treatments were initiated 24 hours after myocardial infarction (MI) and continued to 28 days. Treatments consisted of a suspension vehicle (Veh) and BMS-986235 at either 0.3 mg/kg or 3 mg/kg once per day. **(A)** Kaplan-Meier plot of post-infarction survival in mice dosed with Veh (n = 24), 0.3 mg/kg (n = 23) BMS-986235, and 3 mg/kg BMS-986235 (n = 23). **(B)** Representative heart cross-sections by histology depicting the degree of MI. Histomorphometric analysis of **(C)** scar area, **(D)** infarct wall thickness, and **(E)** left ventricular chamber area 28 days after MI. Group sizes: sham (n = 11), Veh (n = 16-17), 0.3 mg/kg BMS-986235 (n = 13-16), and 3 mg/kg BMS-986235 (n = 13-15). Bar graphs show the mean ± SEM. Dunnett's vs Veh: $*P < 0.05$, $**P < 0.01$, $***P < 0.001$. Log-rank test to compare survival curves: $*P < 0.05$.

approaches that limit adverse remodeling, HF incidence remains high in the post-MI population. It is well established that activation of acute inflammation post-MI facilitates the onset of infarct healing. However, unmitigated inflammation can lead to excessive extracellular matrix degradation within the ischemic myocardium, leading to infarct expansion and severe LV remodeling (22). Targeting the resolution of dysregulated inflammation can lead to efficient myocardial healing and scar formation (11,23). We tested the hypothesis that activation of FPR2 with a potent, selective, and orally bioavailable synthetic small molecule agonist (13) could improve outcome in preclinical models of MI.

FPR2 selectivity was defined relative to its related isoform, FPR1. FPR1 has known roles in mediating proinflammatory activation of neutrophils and migration to distressed tissues due to infection, injury, and disease (24). In several instances, FPR1 activation has been shown to be detrimental and drives worsened outcomes in various disease settings (25). Moreover, with chronic FPR1 stimulation, the potential to exacerbate an already dysregulated inflammatory response may promote further disease progression and undermine the capacity to drive inflammation resolution. Interestingly, as shown in prior studies, simultaneous activation of FPR1/2 with dual agonists can improve cardiac structure and function relationships following MI (11,12). In these studies, there were no findings to suggest untoward effects following multiple weeks of dual agonist treatment. In fact, several important proresolution properties were shown to be highly dependent on FPR2, including IL-10 and IL-6 responses as well as respiratory burst activity induced in HL-60 phagocytes (11). Hence, to optimize the proresolution properties of FPR2 and diminish potential proinflammatory processes associated with FPR1

FIGURE 8 Effects of BMS-986235 on Post-Infarction Structure-Function in Rat

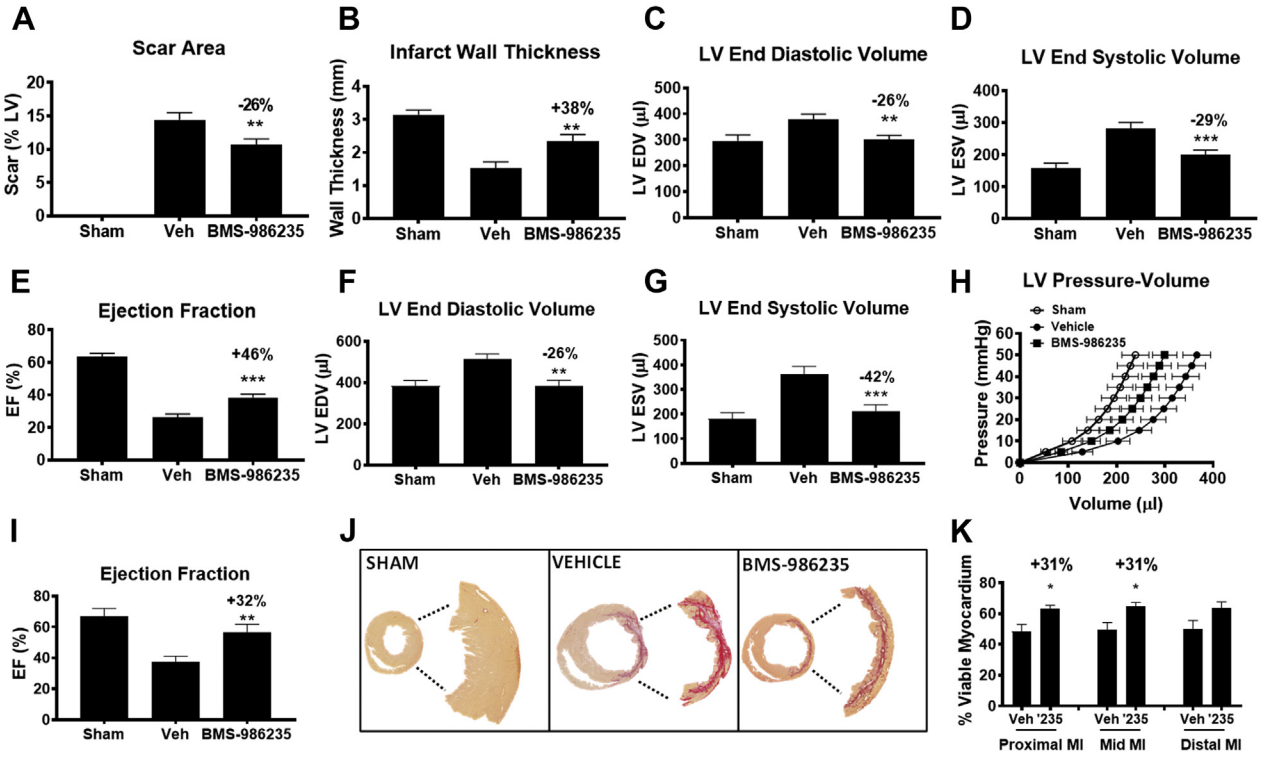

Treatments were initiated 48 hours after myocardial infarction (MI) and continued to 6 weeks. Treatments consisted of a suspension vehicle (Veh) or BMS-986235 (1 mg/kg) once per day. Endpoints evaluated 6 weeks after MI following permanent coronary artery occlusion: histomorphometric analysis of **(A)** scar area and **(B)** infarct wall thickness; echocardiographic measurements of **(C)** LV end-diastolic volume (EDV) and **(D)** LV end-systolic volume (ESV); and **(E)** ejection fraction percentage (EF%). Endpoints evaluated 6 weeks post MI induced via ischemia-reperfusion injury were **(F)** LV EDV, **(G)** LV ESV, **(H)** ex vivo pressure-volume curves, and **(I)** EF%; **(J)** histology of heart and LV infarct cross-sections; and **(K)** regional analysis of viable myocardium across the infarct wall. Group sizes for permanent coronary artery occlusion and ischemia-reperfusion studies: sham (n = 10 for both), Veh (n = 22-25 and n = 14, respectively), and BMS-986235 (n = 20-24 and n = 14, respectively). **(F, G, I)** Data from indwelling pressure-volume conductance catheter measurements. Data represent the mean ± SEM. Dunnett's vs Veh: $*P < 0.05$, $**P < 0.01$, $***P < 0.001$.

activation, a selective FPR2 activation strategy with BMS-986235 was pursued.

The selectivity and proresolution profile of BMS-986235 was confirmed in several key vitro experiments. BMS-986235 selectively activated FPR2-mediated G protein coupling relative to FPR1. BMS-986235-mediated signaling via coupling to Gαi and Gαo is consistent with the known intracellular signaling pathways described for FPR2 (11,26). Moreover, BMS-986235 exhibited potent and FPR2-selective recruitment of β-arrestin1 and 2. FPR2-mediated signaling through β-arrestin1 is reported to be essential for efficient leukocyte migratory function (27). The clearance of apoptotic or necrotic cells by phagocytic macrophages is necessary for inflammation resolution and efficient myocardial wound healing (28). As described previously, peritoneal macrophages from WT mice showed robust enhancements in phagocytosis induced by BMS-986235. The activity was substantially diminished in FPR2-deficient macrophages, indicating a prominent role of FPR2 in driving macrophage phagocytosis. A similar response was observed with zymosan-induced oxidative burst activity, a known response that occurs in activated macrophages following phagosome ingestion (29). Oxidative burst profiles obtained with parental HL-60 cells revealed a concentration-dependent activity pattern with BMS-986235, whereas no response was triggered in FPR2-deficient cells. Similarly, chemotactic responses stimulated by BMS-986235 were highly FPR2-dependent when HL-60 cells were exposed to agonist. These findings were confirmed via the lack of enhanced response using FPR2 deficient HL-60 cells. However, it should

be noted that in the absence of FPR1, HL-60 cells showed reduced oxidative burst efficacy and decreased chemotaxis toward BMS-986235 at higher concentrations, suggesting a more complex interaction that could involve FPR1/FPR2 heterodimers (30).

IL-10 plays an essential role in attenuating proinflammatory responses and enhances the process of inflammation resolution (31). In the setting of experimental MI, increases in IL-10 can potentiate the resolution of myocardial inflammation and improve post-MI cardiac structure and function (23,32). Treatment of isolated human blood with BMS-986235 resulted in concentration-dependent increases in IL-10 gene expression that occurred within hours of compound exposure. Moreover, rodents orally dosed with BMS-986235 showed dose-dependent increases in IL-10 protein levels when challenged with a nonlethal stimulus of LPS. These results demonstrate the predictive and translational nature of the IL-10 response with FPR2 agonism. When rats subjected to MI were treated with BMS-986235, IL-10 levels were shown to increase in the early inflamed myocardial tissue vicinal to the infarct zone. This observation suggests that FPR2 activation with ligands such as BMS-986235 can promote favorable changes in tissue cytokines within key target tissues such as ischemic myocardium. It should also be noted that CD206 levels increased concomitant with IL-10, suggesting an increase in cardiac proresolution macrophages. In addition to IL-10, several important inflammatory cytokines were evaluated in human blood, including MCP-1, IL-6, IL-8, and TNFα. A similar pattern emerged with MCP-1 expression, a cytokine known to regulate the migration and infiltration of monocytes or macrophages into target tissues. By contrast, BMS-986235 did not reveal increases in the proinflammatory cytokines IL-6, IL-8, or TNFα. The cytokine responses characterized in human and rodent blood suggest that FPR2 agonists such as BMS-986235 can evoke detectable changes in the circulation that are consistent with a proresolution profile.

Clearance of apoptotic neutrophils by macrophages (termed efferocytosis) is essential for tissue maintenance and integral to the resolution of inflammation (28,33). A vital step in efferocytosis is the initiation of proapoptotic pathways to enable clearance of dying cells by macrophages. BMS-986235 enhanced in vitro apoptosis of human neutrophils activated with the acute phase protein SAA, a proinflammatory mediator known to extend the lifespan of activated neutrophils (17,30). In vivo, early short-term treatment with BMS-986235 reduced neutrophil levels in post-MI cardiac tissue of mice, suggesting an enhancement in efferocytosis and a concomitant reduction in neutrophil recruitment with FPR2 agonist treatment. Reductions in myocardial neutrophil levels have been observed after MI in mice following treatment with the endogenous FPR2 ligand resolvin D1 (34,35). Additional evidence that BMS-986235 promotes proresolution properties comes from an evaluation of cardiac macrophages in the same 3-day post-MI study. Increases in proresolution marker arginase-1 in the MI border zone and CD206 surface levels in global cardiac macrophage populations from post-MI mouse hearts were observed with BMS-986235 treatment. These findings are consistent with the proresolution stimulatory effects of endogenous proresolution ligands (34,35). Together, these findings support the concept that FPR2 activation by BMS-986235 can potentiate proresolution activities via effects on neutrophil and macrophage populations.

We demonstrate that daily treatment with BMS-986235 improves cardiac structure/function in mouse and rat permanent coronary artery occlusion and rat I/R MI models. The mouse MI model, if left untreated, aggressively remodels the LV and leads to a mortality that averages ~30% to 60%, which typically takes place in the first week after infarction (36). Treatment of mice with BMS-986235 at 3 mg/kg led to a substantial reduction in mortality, suggesting that early pathophysiological events can be targeted to improve outcomes. With 4 weeks of treatment, BMS-986235 reduced infarct scar size by ~55% at the dose of 3 mg/kg relative to vehicle. This was associated with attenuation of LV remodeling as indicated by the preservation of infarct wall thickness and reduction of LV chamber size versus vehicle. These changes occurred concomitant with early enhancement of collagen at the infarct site with BMS-986235 treatment. To confirm the effects observed in the mouse, a comparable MI protocol was implemented in rats. Following 6 weeks of BMS-986235 treatment, rats had smaller infarcts (-26% vs vehicle) and thicker infarct walls (+38% vs vehicle). LV remodeling was attenuated, as indicated by reduced LV volumes at end-diastole and end-systole, and systolic LV function was improved +46% relative to infarcted rats treated with vehicle. Thus, BMS-986235 has the capacity to exert protective effects in two rodent species undergoing a severe form of myocardial injury.

In the clinical setting, the goal is to treat acute MI patients with prompt reperfusion therapy, which is known to salvage myocardium and limit adverse remodeling. We tested the activity of BMS-986235 in an analogous model of MI caused by I/R in the rat in

which it was shown that 6 weeks of BMS-986235 treatment also attenuated LV remodeling and improved systolic LV function. In this model, BMS-986235 also increased viable myocardium levels across the infarct wall, indicating that BMS-986235 treatment was associated with the preservation of functional myocardium. The results obtained with BMS-986235 in these chronic models of HF development indicate that targeted activation of FPR2 has clear cardioprotective activity.

BMS-986235 exerts favorable effects on 2 important aspects of resolution biology. The first is the activation of proapoptotic pathways in proinflammatory neutrophils, which is a prerequisite for inflammation resolution (31). Enhanced clearance of apoptotic and necrotized cells primes the injury site for efficient wound healing and productive scar formation post MI. Optimal healing requires the action of inflammation resolution processes to inhibit further proinflammatory cytokine release, clear inflammatory cell infiltrates, and drive collagen production to produce a stable scar (37). The second is the polarization of macrophages for enhanced phagocytosis. These processes potentiate resolution of adverse unregulated inflammation at times in which post-MI inflammatory cell infiltrates are highest (11,38). Furthermore, the capacity of BMS-986235 to enhance cell migration and stimulate release of the monocyte chemotactic cytokine MCP-1 would also likely serve to recruit and increase the presence of proresolution macrophages for wound healing.

As detailed in this report, the improvements in infarct and LV structure were obtained when therapeutic intervention was given early following MI (24-48 hours after). Intervention at later times post MI and the duration of therapy to yield improved outcomes remain to be addressed. These are important considerations for designing optimal treatment regimens to support clinical studies in the post-MI patient. It is recognized that low-grade inflammation persists as part of the remodeling process and is postulated to contribute to structural changes associated with HF (39,40). This chronic source of inflammation represents a cellular pool for further polarization to drive proper scar maturation and remodeling. Thus, longer-term treatment beyond the early phases of wound healing may be highly beneficial.

STUDY LIMITATIONS. Studies in isolated cell systems that overexpress FPRs may not fully recapitulate the complexity of immune cell responses. And although rodent MI models progress to HF, certain features may not be fully reflective of human disease.

CONCLUSIONS

The findings reported herein demonstrate that pharmacologically activating FPR2 with BMS-986235 can diminish the adverse infarct and LV remodeling that leads to cardiac dysfunction and HF following MI. Our results suggest that pharmacological approaches to activate FPR2 may offer benefit to post-MI patients. This raises the intriguing possibility that proresolution mechanisms, and more precisely, FPR2-targeted strategies, may work in a complementary manner with current standard-of-care therapies to improve survival, infarct healing, and overall post-MI outcome. BMS-986235 was advanced to phase 1 safety trials in healthy subjects (NCT03335553). Clinical studies with BMS-986235 and other FPR2 agonists in post-MI patients will help address the exciting potential of this novel therapeutic approach.

ACKNOWLEDGMENTS The authors thank their colleagues at Kyorin for careful review of the manuscript and for provision of BMS-986235 supporting these studies.

FUNDING SUPPORT AND AUTHOR DISCLOSURES

This work was supported by Bristol Myers Squibb (Princeton, New Jersey, USA). All authors are employees of Bristol Myers Squibb or affiliates via collaboration or contract research.

ADDRESS FOR CORRESPONDENCE: Dr. Ricardo A. Garcia, Bristol Myers Squibb, 3551 Lawrenceville Road, Princeton, New Jersey 08540, USA. E-mail: ricardo.garcia@bms.com.

PERSPECTIVES

COMPETENCY IN MEDICAL KNOWLEDGE: These studies demonstrate the beneficial effects of a selective FPR2 agonist in the setting of post-MI injury. Treatment promoted a proresolution biological profile (cellular function, wound healing, cytokine responses, and gene signatures). Importantly, FPR2 agonist therapy improved LV structure and function in rodent MI models (permanent coronary artery occlusion and I/R injury), demonstrating the importance of the resolution process in improving post-MI outcome.

TRANSLATIONAL OUTLOOK: Efficacy with FPR2 agonist treatment in animal models of MI provides proof of principle for future studies of this mechanism in the post-MI patient population.

REFERENCES

1. Adamo L, Rocha-Resende C, Prabhu SD, Mann DL. Reappraising the role of inflammation in heart failure. *Nat Rev Cardiol*. 2020;17:269–285.

2. Hammerman H, Kloner RA, Hale S, Schoen FJ, Braunwald E. Dose-dependent effects of short-term methylprednisolone on myocardial infarct extent, scar formation, and ventricular function. *Circulation*. 1983;68:446–452.

3. Roberts R, DeMello V, Sobel BE. Deleterious effects of methylprednisolone in patients with myocardial infarction. *Circulation*. 1976;53:I204–I206.

4. Saito T, Rodger IW, Hu F, Robinson R, Huynh T, Giaid A. Inhibition of COX pathway in experimental myocardial infarction. *J Mol Cell Cardiol*. 2004;37:71–77.

5. Mann DL, McMurray JJV, Packer M, et al. Targeted anticytokine therapy in patients with chronic heart failure: results of the Randomized Etanercept Worldwide Evaluation (RENEWAL). *Circulation*. 2004;109:1594–1602.

6. Serhan CN, Chiang N, Dalli J. The resolution code of acute inflammation: novel pro-resolving lipid mediators in resolution. *Semin Immunol*. 2015;27:200–215.

7. Kotwal GJ, Chien S. Macrophage differentiation in normal and accelerated wound healing. *Results Probl Cell Differ*. 2017;62:353–364.

8. Prieto P, Cuenca J, Través PG, Fernández-Velasco M, Martín-Sanz P, Boscá L. Lipoxin A4 impairment of apoptotic signaling in macrophages: implication of the PI3K/Akt and the ERK/Nrf-2 defense pathways. *Cell Death Differ*. 2010;17:1179–1188.

9. Serhan CN, Fiore S, Brezinski DA, Lynch S. Lipoxin A4 metabolism by differentiated HL-60 cells and human monocytes: conversion to novel 15-oxo and dihydro products. *Biochemistry*. 1993;32:6313–6319.

10. Sun YP, Oh SF, Uddin J, et al. Resolvin D1 and its aspirin-triggered 17R epimer: stereochemical assignments, anti-inflammatory properties, and enzymatic inactivation. *J Biol Chem*. 2007;282:9323–9334.

11. García RA, Ito BR, Lupisella JA, et al. Preservation of post-infarction cardiac structure and function via long-term oral formyl peptide receptor agonist treatment. *J Am Coll Cardiol Basic Trans Science*. 2019;4:905–920.

12. Qin CX, May LT, Li R, et al. Small-molecule-biased formyl peptide receptor agonist compound 17b protects against myocardial ischaemia-reperfusion injury in mice. *Nat Commun*. 2017;8:14232.

13. Asahina Y, Wurtz NR, Arakawa K, et al. Discovery of BMS-986235/LAR-1219: a potent formyl peptide receptor 2 (FPR2) selective agonist for the prevention of heart failure. *J Med Chem*. 2020;63:9003–9019.

14. Gallagher R, Collins S, Trujillo J, et al. Characterization of the continuous, differentiating myeloid cell line (HL-60) from a patient with acute promyelocytic leukemia. *Blood*. 1979;54:713–733.

15. Christophe T, Karlsson A, Dugave C, Rabiet MJ, Boulay F, Dahlgren C. The synthetic Peptide Trp-Lys-Tyr-Met-Val-Met-NH2 specifically activates neutrophils through FPRL1/lipoxin A4 receptors and is an agonist for the orphan monocyte-expressed chemoattractant receptor FPRL2. *J Biol Chem*. 2001;276:21585–21593.

16. Liang TS, Wang JM, Murphy PM, Gao JL. Serum amyloid A is a chemotactic agonist at FPR2, a low-affinity N-formylpeptide receptor on mouse neutrophils. *Biochem Biophys Res Commun*. 2000;270:331–335.

17. Ye RD, Sun L. Emerging functions of serum amyloid A in inflammation. *J Leukoc Biol*. 2015;98:923–929.

18. El Kebir D, József L, Khreiss T, et al. Aspirin-triggered lipoxins override the apoptosis-delaying action of serum amyloid a in human neutrophils: a novel mechanism for resolution of inflammation. *J Immunol*. 2007;179:616–622.

19. El Kebir D, József L, Filep JG. Opposing regulation of neutrophil apoptosis through the formyl peptide receptor-like 1/lipoxin A 4 receptor: implications for resolution of inflammation. *J Leukoc Biol*. 2008;84:600–606.

20. El Kebir D, József L, Pan W, et al. 15-epi-lipoxin A4 inhibits myeloperoxidase signaling and enhances resolution of acute lung injury. *Am J Respir Crit Care Med*. 2009;180:311–319.

21. Martinez-Pomares L. The mannose receptor. *J Leukoc Biol*. 2012;92:1177–1186.

22. Shinde AV, Frangogiannis NG. Fibroblasts in myocardial infarction: a role in inflammation and repair. *J Mol Cell Cardiol*. 2014;70:74–82.

23. Jung M, Ma Y, Iyer RP, et al. IL-10 improves cardiac remodeling after myocardial infarction by stimulating M2 macrophage polarization and fibroblast activation. *Basic Res Cardiol*. 2017;112:33.

24. He HQ, Ye RD. The formyl peptide receptors: diversity of ligands and mechanism for recognition. *Molecules*. 2017;22:455.

25. Vacchelli E, Le Naour J, Kroemer G. The ambiguous role of FPR1 in immunity and inflammation. *Oncoimmunology*. 2020;9:1760061.

26. Zhuang Y, Liu H, Edward Zhou X, et al. Structure of formylpeptide receptor 2-Gi complex reveals insights into ligand recognition and signaling. *Nat Commun*. 2020;11:885.

27. Gabl M, Holdfeldt A, Sundqvist M, Lomei J, Dahlgren C, Forsman H. FPR2 signaling without β-arrestin recruitment alters the functional repertoire of neutrophils. *Biochem Pharmacol*. 2017;145:114–122.

28. Horckmans M, Ring L, Duchene J, et al. Neutrophils orchestrate post-myocardial infarction healing by polarizing macrophages toward a reparative phenotype. *Eur Heart J*. 2017;38:187–197.

29. Forman HJ, Torres M. Reactive oxygen species and cell signaling: respiratory burst in macrophage signaling. *Am J Respir Crit Care Med*. 2002;166:S4–S8.

30. Cooray SN, Gobbetti T, Montero-Melendez T, et al. Ligand-specific conformational change of the G-protein-coupled receptor ALX/FPR2 determines proresolving functional responses. *Proc Natl Acad Sci U S A*. 2013;110:18232–18237.

31. Iyer SS, Cheng G. Role of interleukin 10 transcriptional regulation in inflammation and autoimmune disease. *Crit Rev Immunol*. 2012;32:23–63.

32. Krishnamurthy P, Rajasingh J, Lambers E, Qin G, Losordo DW, Kishore R. IL-10 inhibits inflammation and attenuates left ventricular remodeling after myocardial infarction via activation of STAT3 and suppression of HuR. *Circ Res*. 2009;104:e9–e18.

33. Greenlee-Wacker MC. Clearance of apoptotic neutrophils and resolution of inflammation. *Immunol Rev*. 2016;273:357–370.

34. Kain V, Ingle KA, Colas RA, et al. Resolvin D1 activates the inflammation resolving response at splenic and ventricular site following myocardial infarction leading to improved ventricular function. *J Mol Cell Cardiol*. 2015;84:24–35.

35. Halade GV, Kain V, Serhan CN. Immune responsive resolvin D1 programs myocardial infarction-induced cardiorenal syndrome in heart failure. *FASEB J*. 2018;32:3717–3729.

36. Gao XM, Ming Z, Su Y, et al. Infarct size and post-infarct inflammation determine the risk of cardiac rupture in mice. *Int J Cardiol*. 2010;143:20–28.

37. Frantz S, Bauersachs J, Ertl G. Post-infarct remodelling: contribution of wound healing and inflammation. *Cardiovasc Res*. 2009;81:474–481.

38. Nahrendorf M, Pittet MJ, Swirski FK. Monocytes: protagonists of infarct inflammation and repair after myocardial infarction. *Circulation*. 2010;121:2437–2445.

39. Prabhu SD, Frangogiannis NG. The biological basis for cardiac repair after myocardial infarction. *Circ Res*. 2016;119:91–112.

40. Devaux B, Scholz D, Hirche A, Klovekorn WP, Schaper J. Upregulation of cell adhesion molecules and the presence of low grade inflammation in human chronic heart failure. *Eur Heart J*. 1997;18:470–479.

KEY WORDS formyl peptide receptor 2, FPR2, HF, heart failure, MI, myocardial infarction, resolution

APPENDIX For an expanded Methods section and supplemental tables and figures, please see the online version of this paper.